PROCEEDINGS A

royalsocietypublishing.org/journal/rspa

Research

Cite this article: Fowler AC. 2025 The formation of cave scallops. *Proc. R. Soc. A* **481**: 20250033.
https://doi.org/10.1098/rspa.2025.0033

Received: 14 January 2025
Accepted: 12 March 2025

Subject Areas:
applied mathematics

Keywords:
scallops, caves, limestone, ice caves

Author for correspondence:
A. C. Fowler
e-mail: andrew.fowler@ul.ie

Electronic supplementary material is available online at https://doi.org/10.6084/m9.figshare.c.7741397.

THE ROYAL SOCIETY PUBLISHING

The formation of cave scallops

A. C. Fowler[1,2]

[1]MACSI, University of Limerick, Limerick, Republic of Ireland
[2]OCIAM, University of Oxford, Oxford, UK

ACF, 0000-0002-2062-6372

We present a mathematical model for the formation of scallops in ice or limestone caves. The mechanism in each case is similar, and is opaquely related to the mechanism for the formation of dunes and drumlins. Turbulent fluid flow over a wavy bed induces a shift of the maximum bed shear stress upstream of the maximum elevation of the bed. The resulting enhanced shear rate causes enhanced melting or dissolution as appropriate upstream, and this causes an instabilty, which takes the form of a travelling wave. Nonlinear evolution of the waves requires a description of flow separation, and this is empirically accommodated in the model by allowing the melt or dissolution rate to depend on the slope angle of the interface. The resulting model predicts the formation of the cusps which are observed.

1. Introduction

As their name suggests, scallops are clam shell-shaped indentations which form regular patterns in the walls of caves, and are commonly seen in limestone caves and ice caves, as shown in figure 1. Illustrations of them in limestone caves can be found in the paper by Bretz [1, p. 729] for example, and Allen [2] provides an example obtained in the laboratory (figure 2). Their regular form suggests they are a consequence of an instability. For ice, this is associated with enhanced melting in the troughs due to the passage of warm air through the cave, while in limestone it is associated with enhanced dissolution in the hollows associated with the passage of slightly acidic groundwater, through the reaction

$$H_2CO_3 + CaCO_3 \rightleftharpoons Ca^{2+} + 2HCO_3^-. \qquad (1.1)$$

As we shall see, both systems can be described by the same model. At first sight, an instability mechanism

Figure 1. Scalloping on an ice cave below the snout of Vernagtferner, Ötztal Alps, Austria. Picture from summer 2007.

is hard to come by. If we focus on ice scallops, then melting is enhanced by rapid air flow; we might expect air flow over a bumpy surface to be slower in the hollows, in which case melting would be lower, and there would be no instability. In fact, we shall find that the instability mechanism is analogous to that which is the apparent cause of dunes. Fluid flow over a bumpy surface causes the maximum shear stress to be shifted upstream of the point of maximum elevation of the surface. This shift is instrumental in causing the instability. In the present case, the increased shear rate upstream causes an enhanced melting, and it is this which drives the instability.

Curl [3] gives an early discussion of scallops (and 'flutes', their two-dimensional counterparts). Allen [2,4] gives an extensive discussion, and identifies their mechanism of formation. He associates flute formation with a particular value of Reynolds number for the overlying fluid flow, and particularly with the phenomenon of separation in the lee of obstacles, an idea developed by Blumberg & Curl [5] and Curl [6]. These authors also carried out laboratory studies of flute and scallop formation.

Thorsness & Hanratty [7,8] initiated the mathematical study of scallop formation. As is the case for dunes, they identified the upstream shift of maximum bed stress as the causative mechanism, and in their first paper they used a particular eddy viscosity model to calculate the phase angle of the mass transfer coefficient relative to that of a sinusoidal bed. Positive phase angles less than 90° correspond to maximum transport rates on the upwards slope upstream of the bed maximum, and on the elevated part, as found by others, e.g. Benjamin [9] or Jackson & Hunt [10]. However, Thorsness & Hanratty [7] suggest that in certain cases this upstream shift can push past 90°, so that it lies in the trough of the wave, and they associate this with a necessary condition for instability. Thorsness & Hanratty [8] use this result to explicitly propose this as a mechanism for instability, but their model is entirely kinematic, and no more sophisticated than Kennedy's [11] early similar attempt to explain dune formation. Hanratty [12] summarizes and reviews this work.

Meakin & Jamtvelt [13] review in a fascinating paper a whole range of geological patterned phenomena caused by dissolution or precipitation, with occasional summaries of theoretical

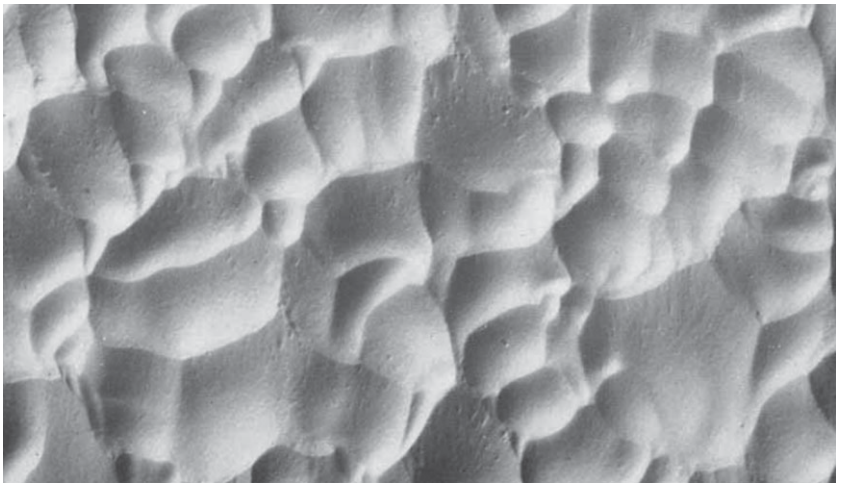

Figure 2. Scalloping in a laboratory experiment of John Allen [2, fig. 2]. Only the lower part of his figure is shown. The flow was from the bottom to the top. The light is shone from the top. The scallops consist of a sequence of pits separated by sharp ridges. The figure can produce an optical illusion where it seems to show a series of mounds, as if the light was shining from the bottom. If this occurs, a way to dispel the illusion is by focusing on a ridge and concentrating on the fact that the light is shining from the top.

explanations. In their discussion of scallops, they point to Blumberg & Curl's [5] qualitative mechanism which resembles Hanratty's, insofar as the maximum dissolution rate occurs in the trough of the scallop, in the recirculation zone of the separated flow over the crest.

Bushuk *et al.* [14] present detailed results of experiments on ice–water scallops. After providing a thorough review of earlier experimental work, much of it from the 1970s, they report their own observations; in particular, they say, in keeping with earlier authors (e.g. [3]), that scallops move downstream, and have an asymmetric profile, with the stoss face being less steep than the lee face (similarly to transverse dunes), though this is less visually clear in their fig. 3. They also provide detailed fluid velocity measurements, showing that a clear separation bubble exists behind the crests of the scallops, in which the flow is relatively weak.

Claudin *et al.* [15] give a detailed theoretical model which can explain the instability which forms scallops. They use a mixing length turbulence model based on Hanratty's work for the turbulent flow, in which the mixing length is proportional to distance from the boundary, modulated with an exponential term which allows transition to the viscous sub-layer very close to the wall. This exponential term contains a critical Reynolds number. Next, this critical Reynolds number is taken to be variable, depending on a dimensionless quantity $\mathcal{H}$ which itself lags spatially behind a horizontal derivative of the horizontal normal stress, and satisfies a corresponding ordinary differential equation. The model is then supplemented by a scalar transport equation for temperature or salt concentration, as appropriate. Exploration of this turbulence model continues [16–18].

The basis for this approach lies in the experimental and theoretical work of Hanratty and co-workers [19]. Thorsness *et al.* proposed a slightly different perturbative approach to the problem of determining the bed shear stress in fluid flow over a wavy bed to that carried out by Benjamin [9], and they found an improved agreement with experimental results. The comparison between the two approaches has been elaborated by Luchini & Charru [20], and then further by Chedevergne *et al.* [16].

There are two comments to make about this model. One is that it uses a complicated description of turbulence, which, although it is designed to provide a good agreement with experiment, is by its nature empirical. The other is exemplified by Thorsness *et al.*'s experiments,

over a bed of amplitude 0.012 m and wavelength 2 m. Such vanishingly small slopes are far away from the large amplitudes of scallops, where separation inevitably occurs, thus rendering the use of these detailed theories questionable in nonlinear growth theories. Indeed, the approach of these models and their consequent linear stability analysis diverges philosophically from the approach of the present paper, which will actually have nothing to say about turbulence.

Another point is that in Claudin *et al.*'s description, it is hard to see where the prescription of the interfacial growth rate is made. It is not written as an explicit boundary condition. All the ingredients are there, but an explicit Stefan condition is not given. This renders the derivation slightly opaque.

The prevailing idea thus seems to be that the instability which generates scallops is due to the same mechanism which generates dunes in deserts or under water. This mechanism lies in the fact that a turbulent flow over a small bump shifts the position of maximum stress upstream. Mathematical models of this have been described by Benjamin [9] and Jackson & Hunt [10], based, respectively, on assumptions of constant eddy viscosity and Prandtl's mixing length theory. In the case of dune formation, this stress shift upstream increases the sediment transport there. It is then a consequence of the Exner equation that a planar interface will be unstable.

The scallop mechanism cannot be exactly the same, since there is no corresponding Exner equation (there is no interfacial 'bedload' transport), rather the melting or dissolution (in ice or limestone caves, respectively) is simply due to the heat or solute transfer at the interface. It seems that the increase of stress on the upstream face of a bump will also cause an increased heat or solute transfer coefficient, and thus increase melting or dissolution; but this is a stabilizing mechanism, as Thorsness and Hanratty pointed out. It seems that the additional lag in the turbulent mixing length formulation of Claudin *et al.* is what provides a viable mechanism for the instability.

Here we provide a different mechanism, based partly on the observation that scallops form sharp edges (something that none of the previous theories have addressed). It is well known in metallurgy that faceted crystals grow in solidification because the growth rate depends on interfacial orientation [21,22], and the same point has been made in geological systems [23]. The resulting sharp interfaces are shocks (jump discontinuities) in the slope, and this distinguishes scallops from dunes, where there are indeed shocks, but these would be jumps in elevation, were it not for the limit to the slope due to the angle of repose.

The instability mechanism is perhaps similar in concept to that provided by previous authors, insofar as it prescribes a variation of interfacial dissolution rate with spatial position on the scallop, but rather than use Hanratty's [12] eddy viscous lag term or Jackson & Hunt's [10] integral convolution, we simply associate this variation with the slope angle of the interface. This empirical choice has the advantage of enabling greater insight into the mechanism and nonlinear development of the interface shape.

2. Mathematical model

We consider first the case of limestone dissolution. In view of the difficulty that has been the case in determining a mechanism for instability, we propose the simplest possible model that we can. Dissociation of carbonic acid into hydrogen and bicarbonate ions suggests a simpler form of equation (1.1), namely

$$\mathrm{H^+ + CaCO_3} \underset{k_-}{\overset{k_+}{\rightleftharpoons}} \mathrm{Ca^{2+} + HCO_3^-}, \tag{2.1}$$

and the overall rate of reaction, in particular the production of calcium ion $\mathrm{Ca^{2+}}$ is

$$R = k_+[\mathrm{H^+}] - k_-[\mathrm{Ca^{2+}}][\mathrm{HCO_3^-}], \tag{2.2}$$

where the square brackets denote concentrations. In this reaction, we will take $[\mathrm{H^+}]$ and $[\mathrm{HCO_3^-}]$ as constant, so that the reaction rate R is a function of calcium ion concentration $c = [\mathrm{Ca^{2+}}]$, with $\partial R/\partial c < 0$. At an interface, the units of R are mole $\mathrm{m^{-2}\,s^{-1}}$.

To keep matters simple, we take a two-dimensional geometry with downflow coordinate x and transverse coordinate z, and we denote the interface as $z = h(x, t)$, with the solid being in $z < h$. The upwards normal velocity of the interface is then

$$v_n = \frac{h_t}{(1 + h_x^2)^{1/2}} = -V_L R, \tag{2.3}$$

where V_L is the molar volume of $CaCO_3$ (units $m^3\,mole^{-1}$).

Now the dissolution of the interface releases calcium ions into the stream, which we take to be a turbulent flow with a turbulent boundary layer next to the wall (the turbulence is not an essential constituent). The simplest description of conservation of calcium in the boundary layer is to write

$$uc_s = \mu R - \lambda c + Dc_{ss}, \tag{2.4}$$

where u is the fluid velocity. The first three terms in this equation represent, respectively, the advection of calcium in the boundary layer, its source from dissolution, and its release to the main stream. More generally, we might model this as a transverse diffusive term. The units of μ are inverse length, and since equation (2.4) is essentially obtained by integrating across the turbulent boundary layer, μ^{-1} is effectively the boundary layer thickness. Similarly, λc represents the flux to the mainstream divided by the boundary layer thickness.

In this model, we also include a longitudinal diffusive term, which represents the effects of eddy-diffusive transport along the boundary layer. This term is likely to be very small, but is included as it may act to provide a shock structure for any shocks which occur. However, we will mostly ignore it. Note that the spatial coordinate along the boundary layer is arc length s, as is appropriate.

The key additional assumption, and this is where the analogy with dune-forming processes occurs, is to suppose that μ depends on the interface slope $S = h_x$. The reason for this assumption is that dunes are formed through a mechanism whereby the undulations of the interface cause the maximum shear stress of the flow to be shifted upstream from the maximum elevation of the bed. Generally, one finds that the shear stress is a complicated convolution integral of the interface slope, but the implication is made well enough in this simplest of approaches by taking the shear stress to be an increasing function of the slope. Now we can suppose that the shear stress is inversely proportional to the boundary layer thickness, and since so also will the dissolution rate, we can take μ to have a similar dependence as the shear stress on the slope. To be specific, we take $\mu = \mu(S)$ and suppose $\partial\mu/\partial S > 0$.

(a) Linear stability

We can write the reaction term in equation (2.2) in the form

$$R = K(c_{\text{sat}} - c), \tag{2.5}$$

where c_{sat} is the saturation concentration, and we take K to be constant. With $\mu(0) = \mu_0$, the model given by equations (2.3)–(2.5) has a uniform, steadily retreating state in which $\mu_0 R = \lambda c$ defines the constant c_0, and then $h = -v_0 t$, where $v_0 = V_L R_0$, and $R_0 = R(c_0)$.

To study the stability of this state, we write $c = c_0 + C$ and $h = -v_0 t + H$, and then linearize equations (2.3) and (2.4). Note that since $x_s = 1/(1 + h_x^2)^{1/2}$, when the system is linearized, one can replace the s derivatives by x derivatives. The linearized system is then

$$\left.\begin{aligned} H_t &= -V_L R_c C \\ \text{and} \qquad uC_x &= \mu_0 R_c C + \mu_S R_0 H_x - \lambda C, \end{aligned}\right\} \tag{2.6}$$

and we have left off the diffusive term. The partial derivatives R_c and μ_S are evaluated at the steady state.

There are normal mode solutions proportional to $\exp(\sigma t + \mathrm{i}kx)$, and a little algebra shows that

$$\sigma = \frac{\mathrm{i}k\mu_S R_0 V_L |R_c|}{\mu|R_c| + \lambda + \mathrm{i}ku}, \tag{2.7}$$

and if we write $\sigma = r - \mathrm{i}kw$, where r is the growth rate and w is the wave speed, then these are given by

$$\left.\begin{aligned} r &= \frac{\mu_S R_0 u V_L |R_c| k^2}{\{\lambda + \mu|R_c|\}^2 + k^2u^2} \\ \text{and} \qquad w &= -\frac{\mu_S R_0 V_L |R_c|(\mu|R_c| + \lambda)}{\{\lambda + \mu|R_c|\}^2 + k^2u^2}. \end{aligned}\right\} \tag{2.8}$$

From this, we can see that the uniform state is always unstable if $\mu_S > 0$ and $R_c < 0$, and the corresponding waves move upstream. The growth rate grows with the wavenumber but remains finite at large k. This seems to be the usual behaviour in interfacial growth instabilities, where the instability at large wavenumber is associated with the formation of shocks in the underlying hyperbolic model. The influence of the diffusive term Dc_{ss} is easily ascertained in the stability analysis, since the corresponding extra term C_{xx} in equation (2.6) simply has the effect of replacing λ in equation (2.8) by $\lambda + Dk^2$. Thus, the growth rate of the high wavenumber modes decays to zero at large k, but the uniform state is still always unstable.

3. Nonlinear evolution

First we reformulate the model in the following way. We write $\mathbf{r} = (x, h)$, and then the unit tangent and normal vectors are

$$\mathbf{t} = (x_s, h_s) \quad \text{and} \quad \mathbf{n} = (-h_s, x_s), \tag{3.1}$$

and the Serret–Frenet formulae in the present two-dimensional case (with torsion zero) are

$$\mathbf{t}_s = \kappa\mathbf{n} \quad \text{and} \quad \mathbf{n}_s = -\kappa\mathbf{t}, \tag{3.2}$$

where the curvature is

$$\kappa = \frac{h_{ss}}{x_s} = -\frac{x_{ss}}{h_s}. \tag{3.3}$$

The normal velocity condition (equation (2.3)) can be written as $\mathbf{r}_t.\mathbf{n} = -V_L R$, whence we can define

$$\mathbf{r}_t = -V_L R\mathbf{n} - U\mathbf{t}, \tag{3.4}$$

for some function U. If we take the s derivative of this, dot with $\mathbf{t}$, use equation (3.2) and the fact that $\mathbf{t}$ and $\mathbf{n}$ are unit orthogonal vectors, we derive the equation

$$U_s = V_L R\kappa. \tag{3.5}$$

Next we define the complex interface location as $z = x + \mathrm{i}h$, and then equation (3.4) can be written in the form, using equation (3.1),

$$z_t = -(U + \mathrm{i}V_L R)z_s. \tag{3.6}$$

In terms of z, equation (3.3) shows that $\kappa = -\mathrm{i}z_{ss}/z_s$. Further, if θ is the slope angle of the interface (i.e. $h_x = \tan\theta$), then $z_s = \mathrm{e}^{\mathrm{i}\theta}$, so that $\kappa = \theta_s$. If we now take the s derivative of equation (3.6), the model reduces to three coupled equations for θ, c and U:

$$\left.\begin{aligned} \theta_t + U\theta_s &= -V_L R_s, \\ uc_s &= \mu R - \lambda c\ [+Dc_{ss}], \\ \text{and} \qquad U_s &= V_L R\theta_s, \end{aligned}\right\} \tag{3.7}$$

where R is given by equation (2.5), and we take μ as an increasing function of θ.

(a) Non-dimensionalization

It is convenient now to non-dimensionalize the system. We scale the variables as

$$\left.\begin{aligned} &c \sim c_{\mathrm{sat}}, \quad R \sim K c_{\mathrm{sat}}, \quad U \sim V_L K c_{\mathrm{sat}}, \\ \text{and} \quad &s \sim l \equiv \frac{u}{\lambda}, \quad t \sim \frac{u}{\lambda V_L K c_{\mathrm{sat}}}, \quad \mu \sim \mu_0 \end{aligned}\right\} \tag{3.8}$$

(we leave θ as $O(1)$), and this leads to

$$\left.\begin{aligned} R &= 1 - c, \\ \theta_t + U\theta_s &= -R_s, \\ U_s &= R\theta_s \\ \text{and} \quad c_s &= \Gamma \mu R - c \ [+\varepsilon c_{ss}], \end{aligned}\right\} \tag{3.9}$$

where

$$\Gamma = \frac{\mu_0 K}{\lambda} \quad \text{and} \quad \varepsilon = \frac{D}{\lambda l^2}. \tag{3.10}$$

There is another dimensionless parameter which is concealed in the size of $\mu'(\theta)$.

The uniform state is

$$\theta = U = 0, \quad c^* = \frac{\Gamma}{1+\Gamma}, \quad R^* = \frac{1}{1+\Gamma}, \quad \mu = 1, \tag{3.11}$$

and it is straightforward to check that the stability criterion (equation (2.7)) is reproduced (taking $\varepsilon = 0$), with the dimensionless complex growth rate having the form

$$\sigma = \frac{\mathrm{i}kc^*\mu'}{\Gamma + 1 + \mathrm{i}k}. \tag{3.12}$$

If we compare equation (3.12) with equation (2.7), we see that instability requires $\mu'(0) > 0$ and also $c^* > 0$, and thus $\Gamma > 0$. In addition, the term ik in the denominator arises through the term c_s in equation (3.9), and this term is thus also essential to the instability mechanism. We use these observations in the following discussion.

(b) Nonlinear evolution

We will proceed on the assumption that Γ is small. Although we do not offer any clues as to the size of the parameters, this assumption implies that the calcium concentration in the water is far from saturation, and this seems a reasonable assumption.

Since then $c \sim \Gamma \ll 1$, we can take $R \approx 1$ in the equation for c, and then, ignoring the diffusion term and supposing $c \to 0$ as $s \to -\infty$, the solution for c is approximately

$$c = \Gamma \int_0^\infty \mathrm{e}^{-\eta} \mu[\theta(s-\eta, t)] \, \mathrm{d}\eta. \tag{3.13}$$

To be specific, we will initially take $\mu = 1 + \alpha\theta$; then equation (3.13) implies

$$c \approx \Gamma \left[1 + \alpha \int_0^\infty \mathrm{e}^{-\eta} \, \theta(s-\eta, t) \, \mathrm{d}\eta \right], \tag{3.14}$$

and also $U \approx \theta$ (taking $U = 0$ when $\theta = 0$), and θ approximately satisfies

$$\theta_t + \theta\theta_s = 0. \tag{3.15}$$

We thus see that an irregular profile for θ will evolve to form shocks in which the slope jumps down; these are the scallops with their sharp edges. It is tempting to apply a Rankine–Hugoniot condition to equation (3.15) to determine the shock speed, but this is hazardous as the equation

is not derived from an integral conservation law. Instead, we need to identify a suitable diffusion term which can provide a shock structure.

However, the loss of Γ means that equation (3.15) lacks the mechanism of instability. In order to retain it, we retrace our steps, but now holding on to the $O(\Gamma)$ terms where they matter (but not everywhere). So again, $R_s = -c_s$, and we retain this small term on the right-hand side of the equation for θ (because it promotes instability), but ignore it in determining U (because it does not), thus still $U \approx \theta$. With the amended expression for R_s, the equation for θ is modified to

$$\theta_t + \theta\theta_s = \alpha\Gamma \int_0^\infty \mathrm{e}^{-\eta}\, \theta_s(s-\eta, t)\, \mathrm{d}\eta. \tag{3.16}$$

We can repeat the stability calculation for the uniform solution $\theta = 0$ of this equation, and the result is

$$\sigma = \frac{\mathrm{i}k\alpha\Gamma}{1 + \mathrm{i}k}; \tag{3.17}$$

since $\alpha = \mu'(0)$, this is just the small Γ expansion of equation (3.12), which suggests that the selective approximation is appropriate.

(c) Shock structure

The model equation (3.16) is similar in structure to an equation used by Fowler [24] to study the evolution of dunes. The uniform state is unstable due to the integral term, and the advective terms cause the initial periodic perturbations to evolve into periodic shock waves, much as happens in the formation of roll waves [25–28]. To illustrate the consequence, suppose that $\theta = as$ for $s \in (-L, L)$, and is then repeated periodically. Since $h_s = \sin\theta$ and $x_s = \cos\theta$, the interface shape takes the form of an arc of a circle, repeated periodically, providing $aL < \pi/2$. These are thus two-dimensional scallops.

The shocks in θ correspond to jumps in the slope of the interface, and one naturally wonders what the diffusive mechanism is, which will provide a shock structure. Our attention is first drawn to the previously neglected diffusion term in c, but one quickly finds that its inclusion does not provide any shock structure.

In other interfacial growth problems, surface energy plays the rôle of a diffusive term, and that is also the case here. There is a direct dependence of the dissolution rate R on curvature [29] through the influence of the surface energy on the solubility c_{sat}. Specifically [30,31], for small surface energy we have

$$c_{\mathrm{sat}} \approx c^0_{\mathrm{sat}} \left[1 - \frac{V_L\gamma\kappa}{\mathcal{R}T}\right], \tag{3.18}$$

where c^0_{sat} is the solubility for a flat interface, γ is surface energy, $\mathcal{R}$ is the gas constant, and T is the absolute temperature. The negative sign in this equation is because we are measuring curvature from the liquid side.

Assuming the correction term is small, that is,

$$\delta = \frac{V_L\gamma}{\mathcal{R}Tl} \ll 1, \tag{3.19}$$

then the corresponding modification to the definition of R in equation (3.9) is

$$R = 1 - c - \delta\theta_s, \tag{3.20}$$

and then our process of selective approximation replaces equation (3.16) by

$$\theta_t + \theta\theta_s = \alpha\Gamma \int_0^\infty \mathrm{e}^{-\eta}\, \theta_s(s-\eta, t)\, \mathrm{d}\eta + \delta\theta_{ss}, \tag{3.21}$$

and the surface energy term does provide the relevant shock structure. As we expect a jump from positive to negative θ at a shock, they can propagate in either direction.

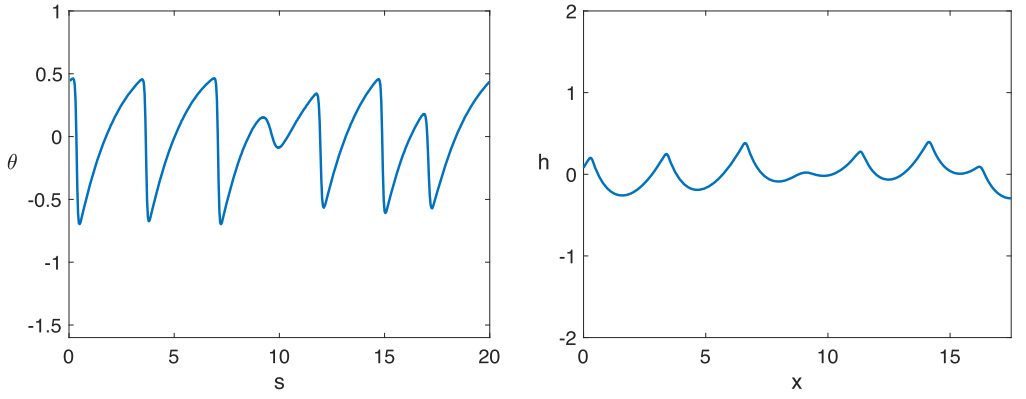

Figure 3. Solution of equation (3.22) using random initial conditions, and parameters $\delta = 0.02$, $\beta = 0.5$; the form of the solution for $\theta(s)$ and $h(x)$ is shown at $t = 20$.

(d) Numerical solution

We have solved the equation

$$\theta_t + \theta\theta_s = \beta \int_0^\infty \mathrm{e}^{-\eta}\theta_s(s-\eta, t)\,\mathrm{d}\eta + \delta\theta_{ss} \tag{3.22}$$

numerically. Figure 3 shows a typical solution, which illustrates the point. θ evolves to a sequence of shock-like waves (these ones move backwards), for which the corresponding interface profile forms scallops with cusped edges.

As was found in a similar model [24], coarsening occurs, although rather slowly, and this may be associated with the spectral method used (the equation is solved with periodic boundary conditions). The code used to obtain the solution is included as electronic supplementary material.

(e) Ice scallops

Although we have framed our model in the context of limestone dissolution, figure 1 illustrates the fact that the same phenomenon occurs in ice caves, and we suppose for similar reasons. We now elaborate this.

We begin with the geometry as in figure 1. The coordinate z points downwards, and we denote the interface as $z = h$ (so we expect scallops as in figure 3). As for equations (2.3) and (2.4), the normal (downwards, in the z-direction) velocity is

$$v_n = \frac{h_t}{(1+h_x^2)^{1/2}} = -M, \tag{3.23}$$

where M is the melt rate. If T is the temperature in the boundary layer and T_a is the (air) temperature in the far field, then an energy equation equivalent to equation (2.4) is

$$\rho_w c_p u T_s = -\rho_i L M - h_a(T - T_a) + k_T T_{ss}, \tag{3.24}$$

where L is latent heat, c_p is specific heat, ρ_i and ρ_w are ice and water densities, respectively, h_a is a far field heat transfer coefficient, and k_T is an eddy thermal conductivity.

The melt rate is determined by the Stefan condition at the interface, and if we suppose the ice is (approximately) isothermal, we can prescribe

$$\rho_i L M = h_T(T - T_M), \tag{3.25}$$

where h_T is a turbulent boundary layer heat transfer coefficient, and T_M is the melting temperature at the interface, which is given by the Gibbs–Thomson relation

$$\frac{\rho_i L(T_M - T_f)}{T_f} = \gamma\kappa, \tag{3.26}$$

where T_f is the reference value for a straight interface, γ is the surface energy, and the curvature κ is measured from the air side of the interface.

Adopting the Serret–Frenet description as before, equations (3.23), (3.25) and (3.26) lead to

$$\left.\begin{aligned} \theta_t + U\theta_s &= -M_s, \\ U_s &= M\theta_s \\ \text{and} \qquad M &= \frac{h_T}{\rho_i L}\left[T - T_f - \frac{\gamma T_f}{\rho_i L}\theta_s\right]. \end{aligned}\right\} \tag{3.27}$$

We make the system (equations (3.27) and (3.24)) dimensionless by scaling the variables as

$$\left.\begin{aligned} T - T_a \sim \Delta T = T_a - T_f, \quad h_T = h_0 K(\theta), \quad M \sim U \sim \frac{h_0 \Delta T}{\rho_i L}, \\ \text{and} \qquad s \sim l = \frac{\rho_w c_p u}{h_a}, \quad t \sim \frac{\rho_i L l}{h_0 \Delta T}, \end{aligned}\right\} \tag{3.28}$$

and the resultant scaled equations are then almost identical to those for the limestone dissolution, under the identification $T = -c$, $M = R$, and

$$\Gamma = \frac{h_0}{h_a}, \quad \delta = \frac{\gamma T_f}{\rho_i L \Delta T l} \quad \text{and} \quad \varepsilon = \frac{k_T}{h_a l^2}. \tag{3.29}$$

Specifically, the dimensionless version of the equations in (3.27) with equation (3.24) is

$$\left.\begin{aligned} \theta_t + U\theta_s &= -M_s, \\ U_s &= M\theta_s, \\ M &= K(\theta)[1 + T - \delta\theta_s] \\ \text{and} \qquad T_s &= -\Gamma M - T + \varepsilon T_{ss}. \end{aligned}\right\} \tag{3.30}$$

The model is not precisely identical because in the case of ice we assume the interface is at the equilibrium melting temperature. However, the stability and nonlinear properties are essentially the same. We can again expect that δ, $\varepsilon \ll 1$, but it seems more likely that Γ will be $O(1)$, or even larger. This makes the model less susceptible to numerical solution, but nevertheless there is little reason to suppose the outcome would be much different.

4. Discussion and conclusion

We have proposed a simple model which has the ability to explain some features of cave scallops. The model envisages flow of water over limestone, or air over ice, and describes the dissolution or melting by means of a turbulent boundary layer in which the calcium concentration (or air temperature) differs from the value in the mainstream, and also from the saturation value at the interface. The feature of the model which promotes the scalloping instability is the enhancement of the boundary layer transport upstream of interface peaks, a feature well known in the theory of dune formation.

However, the nature of the instability is quite different. The eroded material is not transported along the interface as in a dune, but removed to the mainstream flow. The consequence of this interfacial growth instability is that while nonlinear evolution leads to shock formation, it is not

discontinuities in elevation which form (as it would be for dunes in the absence of an angle of repose), but discontinuities in slope; these then produce the cusped ridges which are observed.

The principal purpose of the present paper is to show how the nonlinear development of the interfacial instability can lead to cusp formation as observed in scallops. However, at the root of this development lies the nature of the instability itself. The present model relies on an interfacial source term μR which depends on both concentration c and slope S, such that the partial derivatives $R_c < 0$ and $\mu_S > 0$. The first of these is a natural consequence of the first-order dissolution kinetics, while the second relies on the thinning of the boundary layer upstream of bed elevation peaks. While this is hardly in doubt, the detail of how this simple model represents the real situation certainly deserves further scrutiny. It may be that the present model contains in effect the same mathematical ingredients as the more complicated turbulence model of Claudin *et al.* [15], but it is difficult to say.

(a) Three-dimensionality

The assumption of 'weak saturation' ($\Gamma \ll 1$) in the model allows for its reduction to a form where analytical insight is possible, and also facilitates a straightforward numerical solution. Our model is intended as a proof of concept, and whether its further study is useful is arguable. There are two features of real scallops which loom on the horizon.

The first is their three-dimensionality. What causes this? A unidirectional flow over sand causes transverse dunes; three-dimensional forms such as star dunes require multiple wind directions. In a theory for drumlin formation, the same was true, but a second instability mechanism enabled three-dimensionality to occur [32]. On the other hand, wind over water produces three-dimensionality naturally through a secondary instability. It is therefore possible that a three-dimensional generalization of the present model would produce three-dimensional scallops in a unidirectional flow. Using a phase field model (for warm water flow under ice shelves), Perissuti *et al.* [33] were able to obtain three-dimensional spatial structures, but these do not resemble scallops. Presumably, the patterns depend on the particular choice of phase field model, but at least it shows that three-dimensionality can occur naturally.

(b) Separation

The second feature, which may impact on the first, is the presence of separation. The flow separates downstream of the ridges, and the same feature in both drumlin and dune formation has caused serious difficulties in the development of the respective theories. Our present simplistic approach artificially avoids the issue by simply associating melt or dissolution rate with the interface angle, but a more realistic model would have to address this issue somehow.

(c) Scallop wavelength

Related to this is the issue of the scallop wavelength l. Curl [3] and Blumberg and Curl [5] promoted the observation that the length of scallops appears to scale consistently with a critical value of the corresponding Reynolds number, on the order of 20,000. Blumberg & Curl reposition this in terms of a Reynolds number

$$Re^* = \frac{u_* l}{\nu} \tag{4.1}$$

based on the friction velocity u_*, finding a critical value in the region of 3000. This association has formed a critical concept in later developments. Claudin *et al.* [15] quote a 1972 paper by Ashton and Kennedy giving experimental data (see their fig. 4b) which confirms the inverse dependence of l on stream velocity u (in the form $l = 0.1/u$).

The theory of Claudin *et al.* obtains this same length scale via the lag derivative in their eqn (2.4), which corresponds to the choice $Re^* = a$, and they take the value $a = 2000$ based on the earlier review of Charru *et al.* [34]. All of these results are based on small amplitude undulations. The implicit idea is that the selected wavelength is that of the linear instability, and then as the

scallops grow, the elevation of their crests will be constrained such that the separation bubble does not quite reach the next crest; thus the linear instability controls the finite amplitude wavelength, despite the fact that the fully developed scallop will have quite a different shear stress signature due to the separation bubble.

The alternative view is expressed by Thomas [35], who associates the wavelength with the size of the recirculating eddies—what he calls the wall similarity hypothesis. In this view, the size of the crests would determine the length of the separation bubble, and thus the scallop length, although how that might be controlled by the turbulent boundary layer is unclear.

(d) Outlook

In conclusion, we propose the present simple model as a pedagogical tool which may facilitate the future development of more realistic models. Its principal purpose has been to provide some insight into the mechanism of finite amplitude scallop formation, at the expense of attempting to incorporate the intricacies of turbulent boundary layer flow. It may be that a bridge can be built between the two approaches, but that must await future developments.

Data accessibility. The code used to obtain the solution is included as electronic supplementary material. The data are provided in electronic supplementary material [36].

Declaration of AI use. I have not used AI-assisted technologies in creating this article.

Authors' contributions. A.F.: conceptualization, data curation, formal analysis, methodology, writing—original draft.

Conflict of interest declaration. I declare I have no competing interests.

Funding. I acknowledge the support of the Mathematics Applications Consortium for Science and Industry (www.macsi.ul.ie) funded by the Science Foundation Ireland mathematics initiative grant no. (06/MI/005).

References

1. Bretz JH. 1942 Vadose and phreatic features of limestone caverns. *J. Geol.* **50**, 675–811. (doi:10.1086/625074)
2. Allen JRL. 1971 Bed forms due to mass transfer in turbulent flows: a kaleidoscope of phenomena. *J. Fluid Mech.* **49**, 49–63. (doi:10.1017/S0022112071001927)
3. Curl RL. 1966 Scallops and flutes. *Trans. Cave Res. Group Great Br.* **7**, 121–160. (doi:10.1090/S0002-9947-1966-0185084-5)
4. Allen JRL. 1971 Transverse erosional marks of mud and rock: their physical basis and geological significance. *Sed. Geol.* **5**, 167–385. (doi:10.1016/0037-0738(71)90001-7)
5. Blumberg PN, Curl RL. 1974 Experimental and theoretical studies of dissolution roughness. *J. Fluid Mech.* **65**, 735–751. (doi:10.1017/S0022112074001625)
6. Curl RL. 1974 Deducing flow velocity in cave conduits from scallops. *NSS Bull.* **36**, 1–5.
7. Thorsness CB, Hanratty TJ. 1979 Mass transfer between a flowing fluid and a solid wavy surface. *AIChE J.* **25**, 686–697. (doi:10.1002/aic.690250415)
8. Thorsness CB, Hanratty TJ. 1979 Stability of dissolving or depositing surfaces. *AIChE J.* **25**, 697–701. (doi:10.1002/aic.690250416)
9. Benjamin TB. 1959 Shearing flow over a wavy boundary. *J. Fluid Mech.* **6**, 161–205. (doi:10.1017/S0022112059000568)
10. Jackson PS, Hunt JCR. 1975 Turbulent wind flow over a low hill. *Quart. J. R. Met. Soc.* **101**, 929–955. (doi:10.1002/qj.49710143015)
11. Kennedy JF. 1963 The mechanics of dunes and anti-dunes in erodible-bed channels. *J. Fluid Mech.* **16**, 521–544. (doi:10.1017/S0022112063000975)
12. Hanratty TJ. 1981 Stability of surfaces that are dissolving or being formed by convective diffusion. *Ann. Rev. Fluid Mech.* **13**, 231–252. (doi:10.1146/annurev.fl.13.010181.001311)
13. Meakin P, Jamtveit B. 2010 Geological pattern formation by growth and dissolution in aqueous systems. *Proc. R. Soc. A* **466**, 659–694. (doi:10.1098/rspa.2009.0189)
14. Bushuk M, Holland DM, Stanton TP, Stern A, Gray C. 2019 Ice scallops: a laboratory investigation of the ice-water interface. *J. Fluid Mech.* **873**, 942–976. (doi:10.1017/jfm.2019.398)
15. Claudin P, Durán O, Andreotti B. 2017 Dissolution instability and roughening transition. *J. Fluid Mech.* **832**, R2. (doi:10.1017/jfm.2017.711)

16. Chedevergne F, Stuck M, Olazabal-Loumé M, Couzi J. 2023 About the role of the Hanratty correction in the linear response of a turbulent flow bounded by a wavy wall. *J. Fluid Mech.* **967**, A39. (doi:10.1017/jfm.2023.507)
17. Stuck M, Chedevergne F, Olazabal-Loumé M, Couzi J. 2024 Influence of the turbulent closure for the prediction of the linear response of a flow bounded by a corrugated wall. *Eur. J. Mech. B/Fluids* **105**, 275–284. (doi:10.1016/j.euromechflu.2024.01.015)
18. Stuck M, Olazabal-Loumé M, Couzi J, Chedevergne F. 2022 On the role of turbulence in scallops formation on the ablative heat shield of a reentry vehicle. In *2nd Int. Conf. on Flight Vehicles, Aerodynamics and Re-entry Missions Engineering (FAR 2022), Heilbronn, Germany, 19–23 June 2022*. (https://hal.archives-ouvertes.fr/hal-03795920)
19. Thorsness CB, Morrisroe PE, Hanratty TJ. 1978 A comparison of linear theory with measurements of the variation of shear stress along a solid wave. *Chem. Eng. Sci.* **33**, 579–592. (doi:10.1016/0009-2509(78)80020-7)
20. Luchini P, Charru F. 2019 On the large difference between Benjamin's and Hanratty's formulations of perturbed flow over uneven terrain. *J. Fluid Mech.* **871**, 534–561. (doi:10.1017/jfm.2019.312)
21. Flemings MC. 1974 *Solidification processing*. New York, NY: McGraw-Hill.
22. Fowler AC, Holness MB. 2022 Interfacial growth morphologies in dense eutectic crystal mushes. *IMA J. Appl. Math.* **88**, 677–701. (doi:10.1093/imamat/hxad033)
23. Chaigne M, Carpy S, Massé M, Derr J, Courrech du Pont S, Berhanu M. 2023 Emergence of tip singularities in dissolution patterns. *Proc. Natl Acad. Sci. USA* **120**, e2309379120. (doi:10.1073/pnas.2309379120)
24. Fowler AC. 2002 Evolution equations for dunes and drumlins. *Rev. Real Acad. Cienc. Exactas, Físicas y Naturales, Serie A. Mat.* **96**, 377–387.
25. Balmforth NJ, Mandre S. 2004 Dynamics of roll waves. *J. Fluid Mech.* **514**, 1–33. (doi:10.1017/S0022112004009930)
26. Dressler RF. 1949 Mathematical solution of the problem of roll waves in inclined open channels. *Comm. Pure Appl. Maths.* **2**, 149–194. (doi:10.1002/cpa.3160020203)
27. Fowler A. 2011 *Mathematical geoscience*. London, UK: Springer.
28. Jeffreys H. 1925 The flow of water in an inclined channel of rectangular section. *Phil. Mag. (VI)* **49**, 793–807. (doi:10.1080/14786442508634662)
29. Levenson Y, Emmanuel S. 2013 Pore-scale heterogeneous reaction rates on a dissolving limestone surface. *Geochim. Cosmochim. Acta* **119**, 188–197. (doi:10.1016/j.gca.2013.05.024)
30. Correns CW. 1949 Growth and dissolution of crystals under linear pressure. *Discuss, Faraday Soc.* **5**, 267–271. (doi:10.1039/df9490500267)
31. Scherer GW. 2004 Stress from crystallization of salt. *Cement Concrete Res.* **34**, 1613–1624. (doi:10.1016/j.cemconres.2003.12.034)
32. Fannon JS, Fowler AC, Moyles IR. 2017 Numerical simulations of drumlin formation. *Proc. R. Soc. A* **473**, 20170220. (doi:10.1098/rspa.2017.0220)
33. Perissuti D, Marchioli C, Soldati A. 2024 Morphodynamics of melting ice over turbulent warm water streams. *Int. J. Multihase Flow* **181**, 105007. (doi:10.1016/j.ijmultiphaseflow.2024.105007)
34. Charru F, Andreotti B, Claudin P. 2013 Sand ripples and dunes. *Annu. Rev. Fluid Mech.* **45**, 469–93. (doi:10.1146/annurev-fluid-011212-140806)
35. Thomas RM. 1979 Size of scallops and ripples by flowing water. *Nature* **277**, 281–283. (doi:10.1038/277281a0)
36. Fowler AC. 2025 The formation of cave scallops. Figshare. (doi:10.6084/m9.figshare.c.7741397)